Active layer hydrology in an arctic tundra ecosystem: quantifying water sources and cycling using water stable isotopes

Heather M. Throckmorton,[1]* Brent D. Newman,[2] Jeffrey M. Heikoop,[2] George B. Perkins,[2]
Xiahong Feng,[3] David E. Graham,[4] Daniel O'Malley,[2] Velimir V. Vesselinov,[2] Jessica Young,[5]
Stan D. Wullschleger[4] and Cathy J. Wilson[2]

[1] *Department of Earth, Atmospheric, and Planetary Sciences, Massachusetts Institute of Technology, 77 Massachusetts Avenue, Cambridge, MA, 02139, USA*
[2] *Earth and Environmental Sciences Division, Los Alamos National Laboratory, Bikini Atoll Rd., Los Alamos, NM, 87545, USA*
[3] *Department of Earth Sciences, Dartmouth College, 6105 Fairchild, Hanover, NH, 03755-3571, USA*
[4] *Biosciences Division, Oak Ridge National Laboratory, Oak Ridge, TN, 37831, USA*
[5] *International Arctic Research Center, University of Alaska, Fairbanks, AK, 99775, USA*

Abstract:

Climate change and thawing permafrost in the Arctic will significantly alter landscape hydro-geomorphology and the distribution of soil moisture, which will have cascading effects on climate feedbacks (CO_2 and CH_4) and plant and microbial communities. Fundamental processes critical to predicting active layer hydrology are not well understood. This study applied water stable isotope techniques (δ^2H and $\delta^{18}O$) to infer sources and mixing of active layer waters in a polygonal tundra landscape in Barrow, Alaska (USA), in August and September of 2012. Results suggested that winter precipitation did not contribute substantially to surface waters or subsurface active layer pore waters measured in August and September. Summer rain was the main source of water to the active layer, with seasonal ice melt contributing to deeper pore waters later in the season. Surface water evaporation was evident in August from a characteristic isotopic fractionation slope (δ^2H *vs* $\delta^{18}O$). Freeze-out isotopic fractionation effects in frozen active layer samples and textural permafrost were indistinguishable from evaporation fractionation, emphasizing the importance of considering the most likely processes in water isotope studies, in systems where both evaporation and freeze-out occur in close proximity. The fractionation observed in frozen active layer ice was not observed in liquid active layer pore waters. Such a discrepancy between frozen and liquid active layer samples suggests mixing of meltwater, likely due to slow melting of seasonal ice. This research provides insight into fundamental processes relating to sources and mixing of active layer waters, which should be considered in process-based fine-scale and intermediate-scale hydrologic models. Copyright © 2016 John Wiley & Sons, Ltd.

KEY WORDS   active layer; arctic; hydrology; tundra; water isotopes

Received 19 August 2015; Accepted 7 April 2016

INTRODUCTION

Climate change and permafrost degradation in the arctic will significantly alter landscape hydro-geomorphology, resulting in changes in hydrological properties and conditions and redistribution of soil moisture in the active layer (the shallow soil layer above permafrost that undergoes annual freeze–thaw cycles). Our current understanding of fundamental hydrologic processes in high-latitude regions is limited, which complicates future predictions of the trajectory and magnitude of water cycling and active layer soil moisture (Zhang *et al.*, 2000; Helbig *et al.*, 2013; Painter *et al.*, 2013). There have been some efforts to investigate water sources and cycling in arctic ponds (Koch *et al.*, 2014), lakes (Anderson *et al.*, 2013) and rivers (Walvoord *et al.*, 2012; Blaen *et al.*, 2014), but few studies report on active layer surface water and subsurface pore waters (Woo *et al.*, 2008; Helbig *et al.*, 2013). Considering the importance of active layer hydrology on plant and microbial communities, geochemistry and biogeochemistry in arctic environments (Fiedler *et al.*, 2004; Newman *et al.*, 2015), understanding active layer hydrologic processes will be critical under projected climate change scenarios, as soil moisture largely determines the energy budget and the form and magnitude of C released to the atmosphere (Aleina *et al.*, 2013; Natali *et al.*, 2015).

*Correspondence to: Heather M. Throckmorton, Department of Earth, Atmospheric, and Planetary Sciences, Massachusetts Institute of Technology, 77 Massachusetts Avenue, Cambridge, MA 02139, USA.
E-mail: heather.throckmorton@gmail.com

In high-latitude regions, soil moisture is highly variable from year to year, and sources of water to the active layer are not well understood nor well represented by hydrologic models (Zhang *et al.*, 2000; Painter *et al.*, 2013). During winter months, precipitation is stored as snow and is released during a brief (approximately 2 weeks) snowmelt period in May–June while the active layer is still frozen (Woo *et al.*, 2008). The frozen active layer is thought to act as a largely impermeable barrier limiting infiltration of snowmelt water (Cooper *et al.*, 1991; Mendez *et al.*, 1998; Takata and Kimoto, 2000; Bowling *et al.*, 2003). While snowmelt pathways seem to have some predictable patterns relating to terrain and soil properties, these patterns can be highly variable and are not well understood (Marsh, 1999). Very few field-based studies have actually investigated water sources to active layer pore waters (Cooper *et al.*, 1991; Sugimoto *et al.*, 2003). More field-based studies are needed to validate assumptions and inform process-based hydrologic models about sources and pathways of water in the active layer.

After snowmelt, the active layer begins to thaw (approximately from June to September), reaching maximum depth in fall prior to winter freeze-up. Evapotranspiration can play an important role in the water budget in high-latitude regions (Liljedahl *et al.*, 2011), but potential evaporation rates are relatively low; thus, water supplied by summer rain to the active layer is generally retained for relatively long periods (Sugimoto *et al.*, 2003). At the end of fall, soil moisture freezes and is stored as ice until the following summer as another potential source for liquid active layer soil water, in addition to snowmelt and summer rain. Few studies have examined the relative contributions and mixing of these different sources of water to the active layer, leading to discrepancies between simulated and measured hydrologic processes (Zhang *et al.*, 2000).

Water stable isotopes and δ^2H and δ^{18}O ratios serve as a valuable tool for inferring hydrologic processes including evaporation and mixing of water from different sources (Craig, 1961). In this study, we report on active layer water isotopes (δ^2H and δ^{18}O) measured on surface waters and subsurface pore waters of a polygonal landscape in Barrow, Alaska (USA), which is a low-elevation tundra landscape overlying continuous permafrost on the Arctic Coastal Plain. Seasonally frozen active layer ice was also measured from cores collected in May and April of 2012 and 2013, along with deeper permafrost samples (approximately 40- to 60-cm depth). Permafrost samples were differentiated based on ice content as either (1) massive ground ice, with a gravimetric water content exceeding 250%, or (2) textural ice, which is suspended in soil mineral and organic matrices. Isotopic compositions of summer and winter precipitation (including snowmelt) δ^2H and δ^{18}O were measured from 2009 to 2013 as potential water sources to active layer pore waters and massive and textural permafrost ice.

Our objectives were to characterize variations in water stable isotope compositions with depth and, where possible, infer mixing of active layer surface waters and subsurface pore waters potentially sourced from snowmelt, summer precipitation and melting active layer seasonal ice. We also considered snowmelt and summer rain as potential sources to massive and textural permafrost ice. Polygonal terrain represents 5–10% of Earth's land surface (French, 2007; Aleina *et al.*, 2013), yet to our knowledge, ours is the first study to use stable isotopes to examine water sources of liquid active layer pore waters in a polygonal tundra landscape and to consider summer/fall precipitation and seasonal ice as potential sources within active layers. We hypothesized that different sources of water to the active layer would have distinct isotope signatures and that active layer waters would predominantly be a mix of summer precipitation and thawing seasonal ice, with lesser contribution from snowmelt. Results will address fundamental knowledge gaps on the sources of water to the active layer and should be useful to inform process-based fine-scale and intermediate-scale hydrologic models.

METHODS

Site description

All samples were collected in and around the Barrow Environmental Observatory (BEO; Barrow, Alaska, 71.2956°N, 156.7664°W; Figure 1), which lies within the Arctic Coastal Plain. Soils contain an organic layer <40 cm thick overlying silt lacustrine sediments (Bockheim and Hinkel, 2005). Mosses (*Sphagnum*, *Dicranum* and *Polytrichum* spp.), sedges (*Carex aquatilis* and *Eriophorum* spp.) and grasses (*Dupontia fisheri* and *Arctophila fulva*) are the dominant vegetation (Zona *et al.*, 2010).

The Next-Generation Ecosystem Experiments intensive study area of the BEO is located in an interlake area between drained thaw lake basins (DTLBs), characterized by polygonal terrain and DTLBs of different ages. DTLBs form as lakes drain and become vegetated (Billings and Peterson, 1980; Hinkel *et al.*, 2003; Bockheim *et al.*, 2004). Polygonal ground is formed by seasonal freezing and thawing of soils, whereby ice wedges form beneath the soil subsurface, consequently uplifting polygonal edges and creating low-elevation polygonal centres (Figure 2). Over time, melting of ice wedges and subsidence of raised polygonal edges can transform low-centred polygons to polygons with high-elevation centres (Figure 2). In addition to high-centred and low-centred polygons with high-elevation rims and
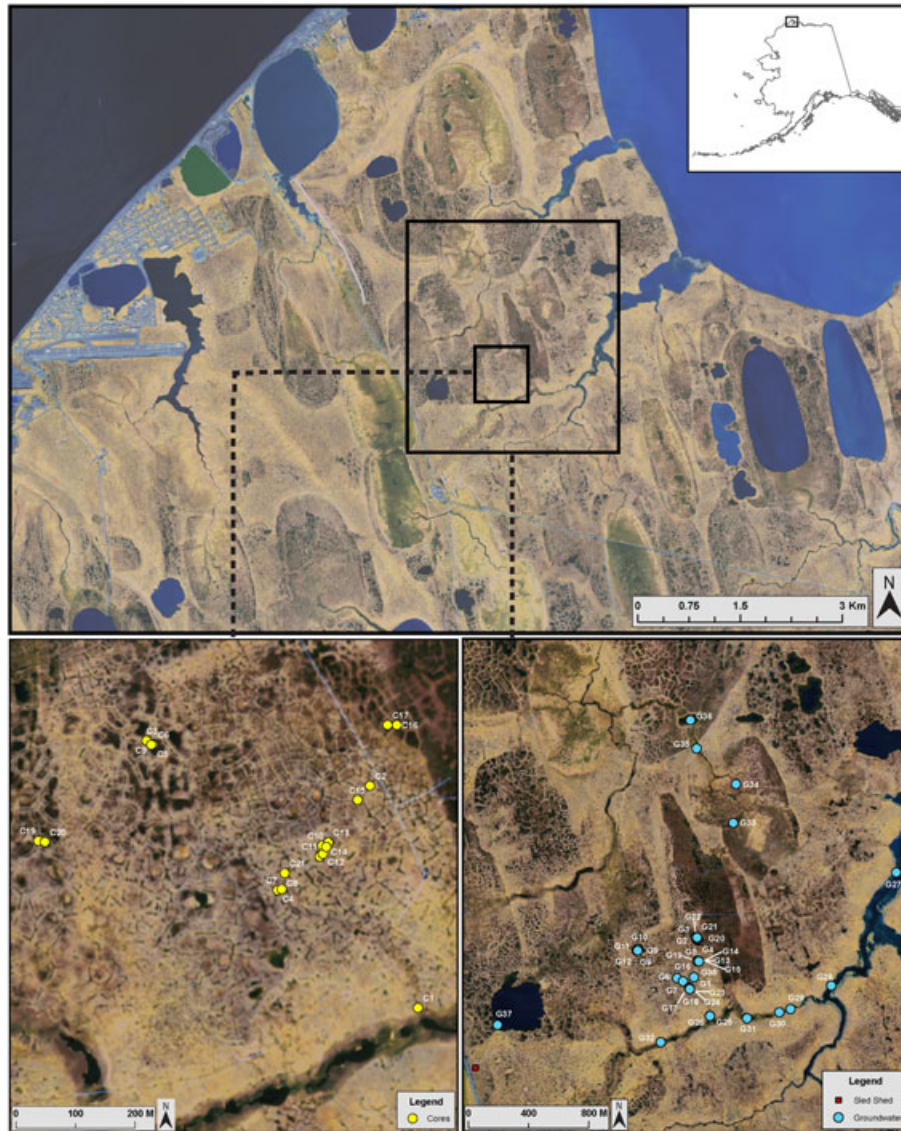
Figure 1. All water isotope samples were collected from Barrow, Alaska (USA). Specific sampling sites for cores and groundwater samples are indicated in yellow and blue circles, respectively. A subset of precipitation samples was collected from the sled shed as indicated in the figure

low-elevation troughs, northern latitude tundra is characterized by hummocky terrain, thermokarst ponds, lakes and wetlands (Arp *et al.*, 2011).

Active layer liquid water collection

Surface and subsurface active layer waters were collected during early August ($n = 21$) and mid-September ($n = 25$) of 2012. Subsurface samples were differentiated as either coming from saturated or unsaturated soils or sediments based on microtopography and water table levels. Unsaturated subsurface samples came from the high-elevation centres of high-centred polygons. Saturated samples came from troughs of high-centred or low-centred polygons, centres of low-centred polygons, ponds or drainage channels (of seasonal rivers or streams).

Surface water samples were obtained by grab sampling and subsurface waters were collected with several techniques. Stainless steel drive point samplers (2.1-cm inner diameter) were installed into shallow saturated soils. A hose was installed into the drive point opening (Masterflex platinum-cured silicone tubing), and water was siphoned into 1-l bottles (high-density polyethylene, Nalgene) using a hand pump vacuum. MacroRhizon samplers (Seeberg-Elverfeldt *et al.*, 2005) were installed into soils, and groundwater was collected into 60-ml syringes. For unsaturated soils, pore water was collected using fibreglass wick samplers (Frisbee *et al.*, 2010).

During August (2012), air temperatures were relatively warm, and precipitation was low relative to the average previous 30-year record (see Table S1). Temperatures for
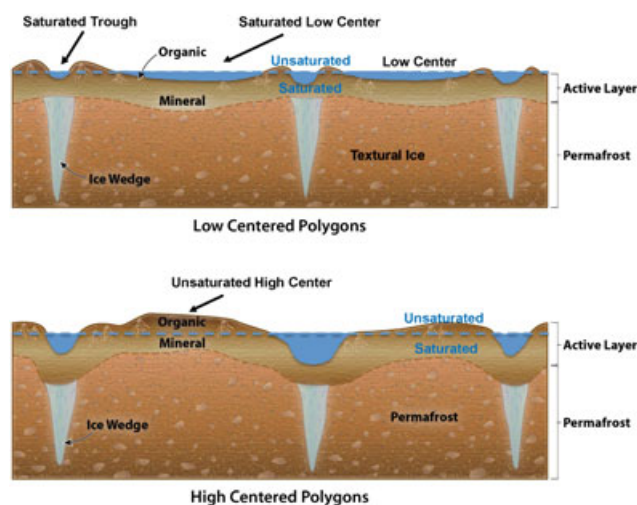
Figure 2. Cartoon cross section of low-centred and high-centred polygons. The blue dashed line in each panel shows the approximate location of the water table and soil saturation, with microtopography above the line representing unsaturated conditions. Areas of solid blue in topographic depressions represent standing water. Base figure courtesy of Yuxin Wu and Susan Hubbard. Revised from Heikoop *et al.* (2015)

August (2012) were 7.2 °C (daily average), −0.5 °C (low mean) and 13.9 °C (high mean), with 28-mm precipitation. Average daily wind speeds were 8 km h^{-1}. September (2012) temperatures were cool relative to the 30-year record, and precipitation was high (Table S1), with a daily average of 0 °C, low mean of −1.6 °C and high mean of 3.9 °C and with 49-mm precipitation. Average daily wind speeds were 8 km h^{-1}. Although relative humidity records were not available for 2012 (August and September), monthly averages for available data from 1995 to 2015 indicate that humidity tends to be similar in August (90 ± 8%) compared with September (87 ± 9%) [National Oceanic and Atmospheric Administration (NOAA) weather station, Barrow, Alaska, USA]. Wind intensities were also similar for August and September in 2012 (NOAA weather station, Barrow, Alaska, USA).

Soil core collection

Cores were collected prior to snowmelt in May and April of 2012 ($n = 6$ cores) and 2013 ($n = 12$ cores) using Snow, Ice and Permafrost Research Establishment augers (Figure 1). Both 5- and 7.6-cm diameter cores were collected from completely frozen soil columns. Snow cover and frozen surface water were cleared from the ground surface prior to core collection. Cores were either collected directly into a polycarbonate liner and placed inside core barrels or collected and immediately transferred to a plastic sleeve following core extraction. Cores were kept frozen and shipped to either the Richmond Field Station (Richmond, CA, USA) or Oak Ridge National Laboratory (Oak Ridge, TN, USA) and stored and processed at −17 °C. Core slices (<5-cm increments)

were subsampled and transported frozen to the Geochemistry and Geomaterials Research Laboratory, Los Alamos National Laboratory (Los Alamos, NM, USA) and stored at −20 °C until analysed. Core subsamples were thawed in airtight containers at room temperature and centrifuged (1 h at 4000 rpm), and solute was decanted and filtered (0.45 μm).

Precipitation and snowmelt collection

One hundred and forty-four precipitation samples were collected for water stable isotope analyses from January 2009 through September of 2013 at the nearby Department of Energy's Atmospheric Radiation Measurment (ARM) Climate Research Facility (Barrow, Alaska, USA), representing all 12 months of the year. A subset of precipitation samples was also collected at the BEO (Figure 1). Precipitation was sampled using a funnel/P-trap/bottle system described by Newman *et al.* (1998), which is effective at preventing post-event sample evaporation. A linear fit of δ^2H *versus* $\delta^{18}O$ was applied to precipitation samples to establish a local meteoric water line (LMWL). A total of 10 snowmelt samples were collected as grab samples during the spring snowmelt period (7 June–10 June 2012).

Laboratory analyses

Water samples, except precipitation samples collected at the ARM facility, were measured for hydrogen and oxygen isotopic ratios using a GV Instruments Isoprime continuous-flow isotope ratio mass spectrometer (IRMS, GV Instruments, Manchester, UK). All stable isotope ratios are reported in the standard δ-notation as the per mil deviation (‰) relative to the Vienna Standard Mean Ocean Water (V-SMOW) for $\delta^{18}O$ and δ^2H. $\delta^{18}O$ and δ^2H values were calibrated using in-house standards calibrated to International Atomic Energy Agency standards V-SMOW, Standard Light Antarctic Precipitation and Greenland Ice Sheet Precipitation. $\delta^{18}O$ was measured through analysis of CO_2 equilibrated for 9 h at 40 °C with 400 μl of water on a GV Instruments Multiflow peripheral instrument. δ^2H was measured using chromium reduction from H_2O using a GV Instruments Eurovector Elemental Analyser. Analytical linearity was monitored and corrected for by analysing standards after every five samples for both methods. Analytical precision on an in-house standard was <±0.20‰ for $\delta^{18}O$ and <±0.99‰ on replicate analyses for δ^2H. The precipitation samples collected at the ARM facility were transported to the Stable Isotope Laboratory of Dartmouth College, where isotopic analyses were conducted using a Delta Plus XL IRMS. For hydrogen isotope measurements, the IRMS was interfaced with an H-device in which water is reduced by reacting with hot chromium. The CO_2

equilibrium method is used for oxygen isotope measurements using a GasBench coupled to the IRMS. The uncertainties of the reported values are within ±0.5 and ±0.1 (one standard error) for δ^2H and δ^{18}O, respectively. Deuterium excess (*d*-excess) was calculated as: *d*-excess $= \delta^2$H $- 8 * \delta^{18}$O (Dansgaard, 1964).

Statistical analyses and isotopic mixing estimates

General linear models were used to test effects described throughout the results section. For numeric predictor variables, we applied Spearman permutation tests (9999 permutations), and one-way analyses of variance tests for nominal variables. Where significant differences occurred, pairwise comparisons were tested for specific differences among variables. We applied Pearson correlation regression analyses to assess linear dependence among variables and to inform linear model analyses. R (v. 2.14.0) was used for all analyses and figures. *p*-values <0.05 are considered significant.

Because of substantial overlap between potential mixing model end members, we utilized a matrix factorization (Lee and Seung, 1999; Alexandrov and Vesselinov, 2014) approach for the isotope mixing model to estimate sources and mixing in the active layer surface and pore waters. The goal of the matrix factorization was to represent the matrix containing the sampling data as the product of two matrices. One of these matrices, *X*, describes the composition of the sources, and the other, *M*, describes the mixing fraction for each source in a given sample.

A constrained optimization methodology was utilized to calibrate *X* and *M*. The following constraints are used:

1. The summer precipitation source should fall on the LMWL.
2. The winter precipitation source should fall on the LMWL.
3. The sum of each row of *M* should be 1.
4. The components of *M* must be between 0 and 1.

The following function is minimized by the optimization routine

$$F(X, M) = \alpha X - X_{0F}^2 + \beta X[-8, 1]^T - E_0^2 + MX - S_F^2$$

where X_0 is the initial guess for the sources' composition (δ^{18}O and δ^2H values for each source), E_0 is the initial guess for the sources' *d*-excess and *S* is the composition of the samples. The first term makes the calibrated sources match the source measurements for δ^{18}O and δ^2H, the second term makes the calibrated sources match the source measurements for *d*-excess and the third term makes the calibrated sources and mixtures match the δ^{18}O and δ^2H values for the samples. The coefficients α and β

were chosen to be 1/100 to reflect the fact that there is greater variation in the sources than in a particular sample. The JUMP (Dunning *et al.*, 2015) modelling language was used to perform the optimization.

Because there is significant variability in the composition of each of the sources (i.e. X_0 and E_0 are uncertain), this induces uncertainty in the mixing estimate, *M*. To address this, we have examined three different initial guesses for X_0 and E_0. One of these initial guesses contains extreme convex hull (i.e. summer with greatest δ^{18}O, winter with least δ^{18}O, etc.) estimates for each of the sources. Another initial guess contains the least extreme estimates for each source such that the convex hull of the sources still nearly contains all of the sampling data. The third initial guess consists of the midway point between the two initial convex hull approaches previously described.

RESULTS

The Global Network for Isotopes in Precipitation (GNIP) database includes δ^2H and δ^{18}O values for 44 precipitation samples collected in Barrow, Alaska, from 1962 to 1969 (year-round; representing all months and seasons; IAEA/WMO, 2015). To our knowledge, no significant datasets for precipitation water isotopes have since been reported for Barrow, Alaska, until now. Barrow annual mean temperature is -11.2 °C, and annual mean precipitation is 113.5 mm (1981–2010). Based on historical climatic records and distinct seasonal trends for daily average temperatures (1974–2012; Table S2; NOAA weather station, Barrow, Alaska, USA), we differentiated four distinct seasons as follows: (1) summer (June–September), (2) fall (October–November), (3) winter (December–March) and (4) spring (April–May). Our precipitation isotope values (δ^2H *vs* δ^{18}O and *d*-excess *vs* δ^{18}O) are plotted with the Barrow GNIP dataset for summer, fall, winter and spring (Figure 3). Pairwise comparisons indicated that water stable isotope values for all seasons significantly differed from each other, with the exception of winter *versus* spring for δ^{18}O ($p = 0.77$), δ^2H ($p = 0.97$) and *d*-excess ($p = 0.10$) and winter *versus* fall for *d*-excess only ($p = 0.92$).

Regression of precipitation isotope values resulted in a LMWL of δ^2H $= 7.5 * \delta^{18}$O $- 1.1$ (compared with the historical GNIP data alone prior to 1969: δ^2H $= 7.1 * \delta^{18}$O $- 9.1$). Our δ^2H and δ^{18}O values combined with the GNIP dataset are not statistically different from the global meteoric water line (δ^2H $= 8.1 * \delta^{18}$O $- 10.8$; Craig, 1961). Precipitation source fields were estimated statistically as presented in Figures 4–6 and were determined based on the δ^{18}O ± 1 standard deviation from the mean (for high and low end members of the source fields), and corresponding δ^2H and
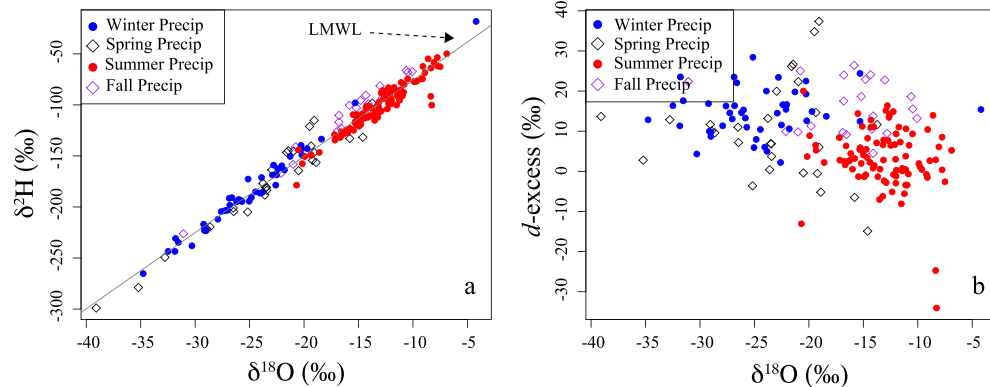
Figure 3. (a) δ^2H–δ^{18}O diagram of precipitation water stable isotope samples. LMWL = local meteoric water line for Barrow, Alaska (USA). (b) d-excess–δ^{18}O diagram of precipitation water stable isotope samples (Barrow, Alaska, USA)
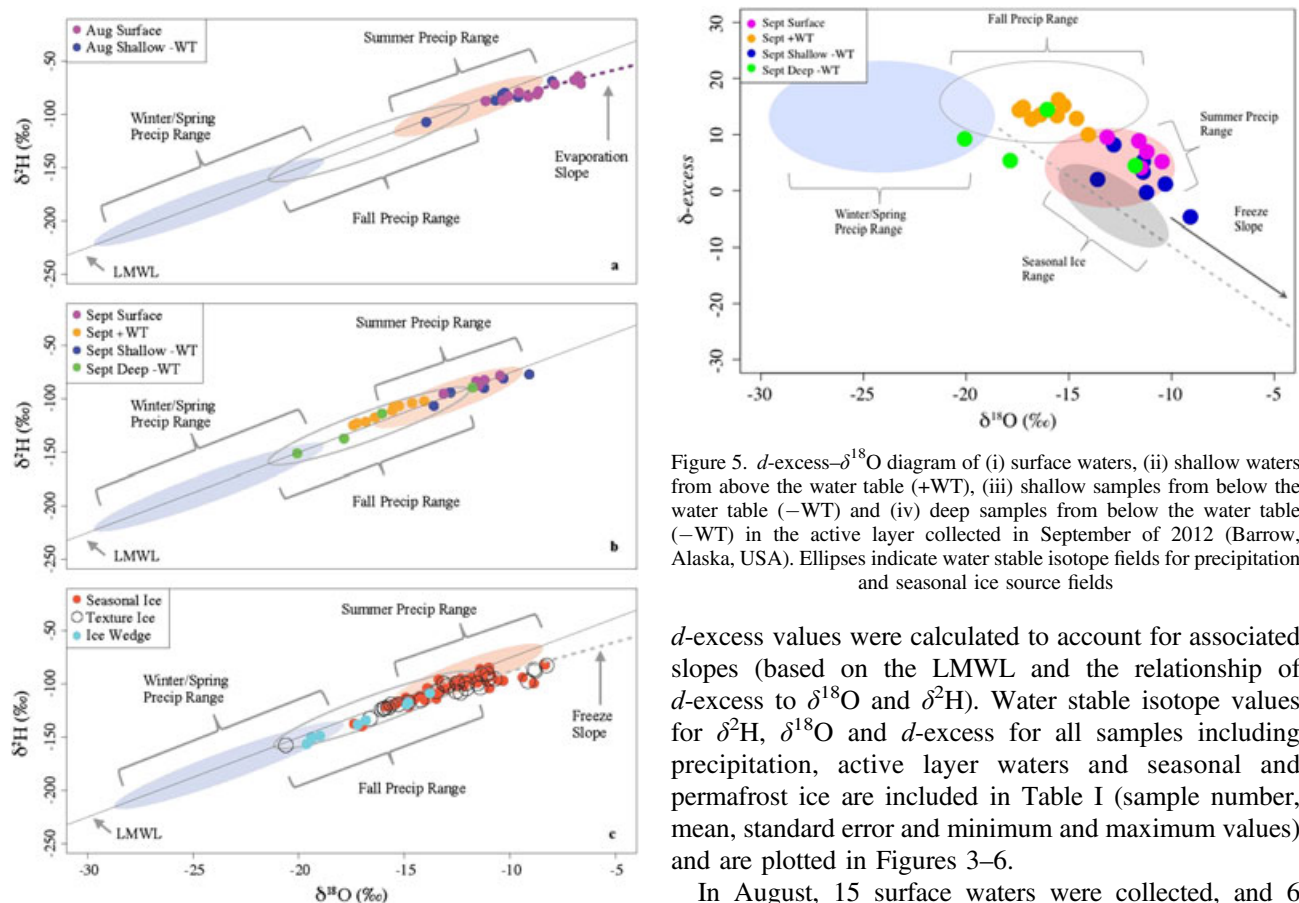

Figure 4. (a) δ^2H–δ^{18}O diagram of surface waters and subsurface waters from the active layer collected in August 2012 (Barrow, Alaska, USA). LMWL = local meteoric water line. The evaporation slope regression estimated from August surface waters is also indicated. Ellipses indicate water stable isotope fields for precipitation source fields. (b) δ^2H–δ^{18}O diagram of (i) surface waters, (ii) shallow waters from above the water table (+WT), (iii) shallow samples from below the water table (−WT) and (iv) deep samples from below the water table (−WT) in the active layer collected in September of 2012. Ellipses indicate water stable isotope fields for precipitation source fields. (c) δ^2H–δ^{18}O diagram of frozen active layer and permafrost samples. The freeze slope regression estimated from seasonal ice is also indicated. Ellipses indicate water stable isotope fields for precipitation source fields
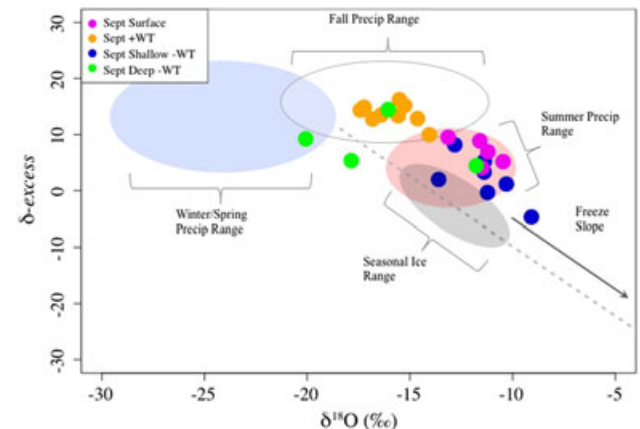

Figure 5. d-excess–δ^{18}O diagram of (i) surface waters, (ii) shallow waters from above the water table (+WT), (iii) shallow samples from below the water table (−WT) and (iv) deep samples from below the water table (−WT) in the active layer collected in September of 2012 (Barrow, Alaska, USA). Ellipses indicate water stable isotope fields for precipitation and seasonal ice source fields

d-excess values were calculated to account for associated slopes (based on the LMWL and the relationship of d-excess to δ^{18}O and δ^2H). Water stable isotope values for δ^2H, δ^{18}O and d-excess for all samples including precipitation, active layer waters and seasonal and permafrost ice are included in Table I (sample number, mean, standard error and minimum and maximum values) and are plotted in Figures 3–6.

In August, 15 surface waters were collected, and 6 samples were collected as saturated subsurface pore waters. No unsaturated subsurface pore waters were collected in August because of sampling difficulties in extracting water. In September, 5 surface water samples were collected, 11 pore water samples were collected from unsaturated subsurface depths (unsaturated centres of high-centred polygons) and 10 pore water samples were collected from saturated subsurface (below the water table from low-elevation microtopographic features). Samples below the water table (collected in September only) were further classified as 'shallow' (<10 cm) or
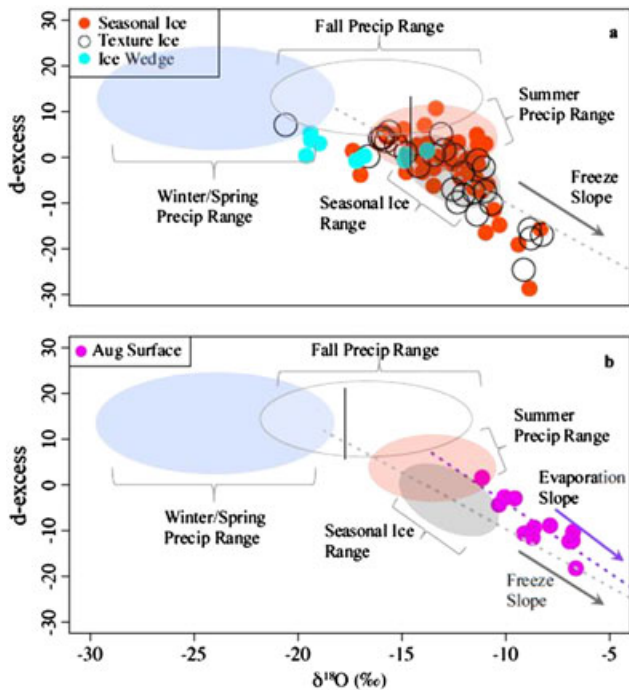
Figure 6. (a) *d*-excess–δ^{18}O diagram of (i) seasonal ice, (ii) textural permafrost ice and (iii) ice wedge permafrost (Barrow, Alaska, USA). The freeze slope regression estimated from textural permafrost ice is also indicated. Ellipses indicate water stable isotope fields for precipitation and seasonal ice source fields. (b) *d*-excess–δ^{18}O diagram of surface waters from the active layer collected in August of 2012 (Barrow, Alaska, USA). The evaporation slope estimated from August surface waters is indicated, as is the freeze slope estimated from seasonal ice. Ellipses indicate water stable isotope fields for precipitation and seasonal ice source fields

'deep' (20–55 cm). Significant differences were found for active layer stable isotopes between the months of August and September ($p < 2.2\mathrm{e}{-16}$ for δ^{18}O, δ^2H and *d*-excess), with September values being more negative for δ^{18}O and δ^2H. Isotope values (δ^2H *vs* δ^{18}O) for August surface waters and August shallow subsurface pore waters (−WT) are plotted in Figure 4a, along with winter/spring, summer and fall precipitation fields. Significant differences in active layer water stable isotopes with depth also occurred ($p < 2.2\mathrm{e}{-16}$ for δ^{18}O, δ^2H and *d*-excess). August surface and subsurface waters primarily plotted along the LMWL within the summer precipitation source field. However, several August surface waters deviated to the right of the LMWL, plotting along an evaporative regression slope of δ^2H $= 5.0\delta^{18}$O $- 34.5$ ($R^2 = 0.89$). The intersection of an evaporation slope (for δ^2H *vs* δ^{18}O) with a meteoric water line (MWL) can be an indicator of the isotopic composition of water prior to isotopic fractionation from evaporation (Souchez *et al.*, 2000). For August surface waters, the evaporation slope intersects the LMWL at δ^{18}O $= -14.6$ and δ^2H $= -129.2$, near the average of the summer precipitation source field (Figure 4a), suggesting a predominantly summer precipitation source for evaporated August surface waters.

September surface water isotopes were significantly more negative than August surface waters and do not show a discernable evaporation effect. Isotope values (δ^2H *vs* δ^{18}O) for September surface waters and

Table I. Water stable isotopes for different sample types (δ^{18}O and δ^2H) and *d*-excess values from in and around the Barrow Environmental Observatory (Barrow, Alaska).

Active layer	*n*	δ^{18}O				δ^2H				*d*-excess			
		Mean	SE	Min	Max	Mean	SE	Min	Max	Mean	SE	Min	Max
Aug. surface	12	−8.6	0.4	−11.2	−6.6	−77.0	2.4	−87.7	−64.4	−8.5	1.6	−18.2	1.5
Aug. shallow	6	−10.5	0.8	−14.0	−8.0	−84.8	5.2	−107.3	−69.0	−0.9	1.8	−7.0	4.4
Sept. surface	5	−11.6	0.4	−13.1	−10.5	−85.7	2.9	−95.6	−78.5	6.9	1.0	4.1	9.5
Sept. (+WT)	10	−15.9	0.3	−17.4	−14.1	−113.4	2.6	−124.9	−102.4	13.8	0.5	10.0	16.2
Sept. (−WT) shallow	7	−11.4	0.6	−13.6	−9.1	−89.1	3.6	−106.8	−77.4	2.1	1.6	−4.7	8.2
Sept. (−WT) deep	4	−16.4	1.8	−20.1	−11.8	−123.1	13.6	−151.4	−89.7	8.4	2.3	4.5	14.4
Seasonal ice	46	−12.8	0.3	−17.4	−8.3	−104.0	1.9	−139.8	−82.3	−1.7	1.1	−28.6	10.8
Permafrost													
Ice wedge	9	−17.2	0.8	−19.6	−13.8	−136.2	5.7	−156.6	−108.8	1.5	0.7	−0.7	5.3
Texture ice	28	−13.0	0.5	−20.6	−8.3	−107.7	3.1	−157.7	−83.0	−3.7	1.6	−24.5	7.1
Precipitation and snowmelt													
Winter precipitation	45	−24.6	0.8	−34.8	−4.2	−182.5	6.5	−265.3	−18.2	14.5	0.9	2.2	28.4
Summer precipitation	91	−13.1	0.3	−20.7	−6.9	−102.0	2.6	−178.6	−49.9	3.2	0.8	−34.1	20.0
Fall precipitation	21	−16.3	1.0	−31.1	−10.1	−113.9	8.3	−226.2	−66.3	16.2	1.4	4.5	26.4
Spring precipitation	28	−23.4	1.1	−39.1	−13.7	−177.6	9.1	−299.0	−98.2	9.9	2.3	−14.9	37.4
Snowmelt (2012)	10	−19.0	0.6	−21.1	−15.3	−143.9	3.9	−160.5	−119.8	7.8	0.8	2.6	10.8

Sample size, mean, standard error (SE), minimum and maximum values shown.

subsurface pore waters are plotted in Figure 4b, along with winter/spring, snowmelt and summer precipitation fields primarily within the summer and fall precipitation fields.

Frozen core sections were identified and classified based on depth, visual inspection of cryogenic structure and ice content and were assigned as seasonal ice (frozen active layer) or permafrost massive/wedge ice *versus* permafrost textural ice. Cores produced a total of 114 seasonal active layer, 47 textural permafrost and 9 wedge ice samples for water isotope analyses (δ^{18}O and δ^2H). Frozen active layer samples (seasonal ice and textural and massive permafrost ice; Figure 4c) had similar trends in water isotope values, with some values plotting along the MWL within winter and summer precipitation fields and some values falling to the right of the MWL. Ice wedge permafrost plotted along the LMWL, mostly within the winter/snowmelt precipitation field, with some values also plotting within the summer precipitation field (Figure 4c). Significant differences in isotopic values occurred for seasonal *versus* ice wedge samples (for δ^{18}O and δ^2H, $p < 2.2e{-}16$); and for textural ice *versus* ice wedge samples (for δ^{18}O and δ^2H, $p < 0.001$), with ice wedge values being more negative for δ^{18}O and δ^2H.

Source mixing results are included in Tables II and III, from four potential sources (winter/spring precipitation, summer rain, fall precipitation and seasonal ice melt). Table II provides the estimates for source water isotope values used in the isotope mixing model (intermediate convex hull source values; optimization discussed in the

Table II. Source value estimates for isotopic mixing model including (i) winter/spring precipitation, (ii) summer rain, (iii) fall rain and (iv) seasonal ice for liquid active layer waters for September active layer waters.

	δ^{18}O	δ^2H	*d*-excess
Winter/spring precipitation	−30.3	−228.6	14.1
Fall precipitation	−15.7	−103.7	21.7
Summer precipitation	−7.3	−55.6	2.5
Seasonal ice melt	−9.4	−93.0	−18.1

Mid-convex hull was used for percentage estimates from different sources.

Table III. Source estimates (%) for September active layer waters including from (i) winter/spring precipitation, (ii) summer rain, (iii) fall rain and (iv) seasonal ice.

	Winter/spring	Fall	Summer	Ice
Surface	5.9	32.2	50.1	11.9
(+WT)	15.8	57.5	19.0	7.8
Shallow (−WT)	6.9	18.4	47.5	27.2
Deep (−WT)	26.4	32.5	24.4	16.6

Section on Statistical Analyses and Isotopic Mixing Estimates). Based on significant overlap with winter and spring precipitation isotope values and the fact that isotope values for these two seasons were not significantly different, winter and spring precipitation values were treated as one potential combined source in isotopic mixing model estimates ('winter/spring'). Source estimates (% contribution) for September surface waters and subsurface active layer pore waters are included in Table III. Water sources for August active layer waters were not quantitatively estimated due to evidence for evaporative isotopic fractionation.

DISCUSSION

General characteristics of stable isotopes in active layer waters

Given the paucity of deuterium and oxygen-18 data on active layer waters, we begin by providing a general characterization of the isotope data collected during this study. Precipitation shows clear seasonality, where winter and spring precipitations have significantly more negative values than summer and fall values (Figure 3a). Snowmelt values are similar to winter/spring values (not significantly different). All values plot along a linear trend typical of meteoric waters, and the Barrow LMWL has a lower slope than the global meteoric water line. However, the local line is not statistically significantly different from the global line, and additional precipitation sampling would be needed to potentially establish a difference.

In August and September, most of the active layer water samples plotted along the LMWL (Figure 4a and b). Some surface water samples from August plotted along a linear trend to the right of the MWL (Figure 4a). The trend has a slope of 5, which is characteristic of surface water evaporation (see Barnes and Allison, 1983, and references therein). The low-relief topography of the Barrow area Arctic Coastal Plain limits lateral run-off of water, resulting in strong evapotranspiration controls on the water budget during the summer (Boike *et al.*, 2008; Liljedahl *et al.*, 2011). The importance of evaporation in these landscapes is supported by Koch *et al.* (2014) who demonstrated substantial volumetric water loss from ponded surface waters in an area about 88 km south-east of our study site during 2012. Stable isotope values also reflected these evaporative losses. The indication of significant evaporation effects in early summer to midsummer based on our study and Koch *et al.* (2014) also suggests that relatively stagnant conditions existed within polygonal ground areas near Barrow, with limited lateral transport of active layer water.

By September, active layer samples no longer showed any evaporative effect, and all samples plotted along the

LMWL. Koch *et al.* (2014) also noted a stronger evaporation signal in early summer compared with late summer. Greater evaporation loss earlier in the season can be explained by the lower precipitation and warmer temperatures that occurred in August relative to September 2012. For example, only 2.8 cm of precipitation occurred in August, compared with 4.9 cm in September (NOAA weather station, Barrow, Alaska, USA). Relative humidity and wind also play a role in evaporation. However, records indicate similar relative humidity and wind intensities for August and September (Section on Methods). Our study did not differentiate among body water sizes or types because of the limited number of sampling locations. However, the size and morphology of surface water bodies play a role in the amount of evaporation loss. For example, Arp *et al.* (2011) showed that larger lakes had more thermokarst erosion and drying, while Koch *et al.* (2014) reported lower evaporation from troughs relative to small ponds and the centres of low-centred polygons. Because of low hydrologic conductivity, hummocks can obstruct drainage (Quinton and Marsh, 1998), and preferential drainage may occur in lower-elevation microtopographic units such as troughs. Quantifying the effects of microtopography and vertical and lateral fluxes was beyond the scope of our study, but preferential drainage may result in some lateral movement of water in surface and subsurface active layer waters.

Another notable characteristic is the significant variation of isotope composition with active layer depth. The depth variation was most apparent during September (deeper samples were not available to fully evaluate depth variations in August). September surface waters and shallow subsurface pore waters below the water table tended to have less negative values, while deep pore waters (near the frost line) and pore waters from above the water table (from the centres of high-centred polygons) tended to have more negative values. The more negative values from the centres of high-centred polygons are somewhat surprising given that these areas are topographic highs, and this aspect is discussed further in the Section on Sources of Active Layer Waters. September active layer thicknesses were typically less than 50 cm, yet isotope stratification developed. Newman *et al.* (2015) found that there was also development of strong geochemical depth gradients within the active layer at the study site in 2012. The presence of well-developed isotope and geochemical gradients within these thin active layers suggests that advective mixing is likely minimal in polygonal ground near Barrow. If significant advection was occurring, it seems unlikely that these depth gradients would be maintained. In tundra peat soils, bulk density tends to increase and porosity tends to decrease with depth (Quinton *et al.*, 2000), and soil layering can result in sharp decreases in hydrologic conductivity with depth

(Quinton *et al.*, 2008). Such decreases with depth would limit advection and help explain the development of distinct isotopic values with depth. In addition, the isotope depth variations suggest that the sources of water may vary within the active layer, and this is explored more fully in the following section.

Sources of active layer waters

There are several potential sources to active layer surface and subsurface pore waters, including (1) meteoric sources (i.e. winter precipitation as snowmelt mixed with spring rain, summer precipitation and fall precipitation) and (2) seasonal active layer ice melt. The August and September active layer water stable isotopes show little evidence of winter/spring/snowmelt contributions to the active layer (Figure 4a and b). Snowmelt has a large effect on arctic and other high-latitude stream and river flows (e.g. Cooper *et al.*, 1991; Streletskiy *et al.*, 2015; Tetzlaff *et al.*, 2015a) and causes substantial flooding of our polygonal ground study site in the spring during peak snowmelt season. However, the almost complete lack of correlation between active layer isotope compositions and the winter/spring precipitation field (Figure 4a and b) suggests the importance of snowmelt as a source of active layer water is minor. The main reason is that during snowmelt there is little to no active layer development and snowmelt rapidly runs off into larger stream channels. In the Barrow area, the snowmelt period typically only lasts 2 or 3 weeks. Thus, the snowmelt period in low-relief areas of the Arctic Coastal Plain represents a time of high surface run-off and lateral transport of snowmelt water (Woo *et al.*, 2008). Infiltration of snowmelt is limited by the volume of ice-filled pores and reduced permeability, and these factors along with vegetation are major controls on how much snowmelt is retained in the soil (Marsh, 1999; Sugimoto *et al.*, 2003; Tetzlaff *et al.*, 2015b). The rapid and transient nature of snowmelt is also supported by stable isotope studies of arctic streams (Cooper *et al.*, 1991; Streletskiy *et al.*, 2015). For example, in a watershed-scale stable isotope study in Alaska, Cooper *et al.* (1991) found that the snowmelt contribution to streamflow was negligible within a month of snowmelt. In a boreal forest study, Sugimoto *et al.* (2003) suggested only about half of snowmelt infiltrated into the shallow surface (approximately 15 cm) of a Siberian taiga larch forest, and this was quickly transpired and lost during leaf unfolding. In contrast, in a sandy pine forest, snowmelt infiltrated to a depth of 120 cm. Their pine forest results suggest that in forested landscapes with coarse-textured soils, snowmelt may be a more important part of the summer water balance than in tundra systems.

In contrast to winter and spring precipitation/snowmelt, summer rainfall appears to be a major contributor to

active layer water. Most of the surface and subsurface pore water isotope values from this study fall directly within the summer precipitation field of the MWL diagram regardless of whether they were collected in August or September (Figure 4a and b). All of the August active layer waters plotted within the summer precipitation field except those that were affected by evaporation. September results were similar except (as noted earlier in the discussion of depth dependence of isotopic variation) for deep samples (below the water table near the frost line) and samples above the water table from high-centred polygons that have more negative values that can extend into the fall precipitation range (Figure 4b). Fall precipitation appears to be an especially strong contributor to the centres of high-centred polygons. A reason for this shift from less summer to more of a fall source is that the high centres can be unsaturated (as they extend above the local polygon water table) and have less accumulated summer water. Because the porosity is not completely filled, there is less isotopic dilution of fall precipitation events (with lower δ^2H and $\delta^{18}O$) compared with troughs and low-centred areas that are fully saturated (with higher δ^2H and $\delta^{18}O$). Because of the elevated topography (Figure 2), there is also a greater likelihood for summer precipitation to drain or run off from the high polygon centres. Inter-hummock and low-centred areas are associated with preferential water accumulation and flow relative to hummock and high-elevation areas (Quinton et al., 2000). We hypothesize that polygonal ground isotope values in unsaturated topographic highs may be more sensitive to recent precipitation inputs than topographic lows. Additional higher-frequency field sampling would be needed to test this hypothesis.

Deep September samples from near the frost line also appear to have a potentially large fall source contribution (Figure 4b). However, such an explanation is problematic because most of the shallow-surface-water and pore water values plot above the fall precipitation field (within the upper part of the summer field). It would take a convoluted set of flow paths for less negative fall water to percolate to depth without shifting the isotope composition of the shallower active layer water. This suggests that another source may be important for the deeper part of the active layer.

The preceding discussion has assumed that most of the active layer source is either summer or fall precipitation. These results seem reasonable given the correspondence of the active layer isotope values with the isotope composition of fall and summer precipitations and the fact that the polygonal ground study site is poorly drained and fall and summer precipitation must be stored on the landscape somewhere. However, this interpretation ignores potential contributions from melting seasonal ground ice as the active layer progressively thickens

during the thaw period. We can make a coarse estimate to understand the potential magnitude of seasonal ice contributions to the active layer using simple constraints of active layer thickness and porosity. We assume an active layer porosity of 74% by volume based on values for a shallow peat layer (peat, 88%) and deeper mineral soil (silty loam, 60%) (Atchley et al., 2015). Assuming fully saturated frozen soil (not accounting for volume differences between ice and liquid water), we estimate that with a 50-cm thaw depth, 37 cm of frozen active layer water could be released as meltwater. In other words, ice melt could fill roughly 50% to nearly 75% of the active layer porosity (depending on actual porosity and ice density variations). For 2012, summer and fall precipitations (June–November) amounted to 9.3 cm (total annual precipitation was 11.1 cm). Although approximate, these estimates suggest that there is a larger potential for active layer water to be derived from ice than to be derived from recent precipitation. However, it is important to note that this estimation approach assumes there is no lateral drainage loss of meltwater. It also ignores the fact that the active layer progressively thaws during the warm season, and so new meltwater will only be added to the active layer as a function of the rate of thaw. It is not all instantaneously present.

In order to clarify the potential role of melting seasonal ice as an active layer source, we measured the isotope values of seasonal ice (Figure 4c). Ice values spanned most of the summer precipitation field with the majority of values plotting on the right side of the LMWL, and some values were so far to the right that they did not plot within the summer precipitation field at all. In terms of constraining an ice melt end member for understanding sources of water in the active layer, there was overlap with the summer precipitation end member, but there were also the distinct ice values that did not plot within the summer precipitation field at all, and these require further discussion. These 'anomalous' values are clearly fractionated, and the degree of difference from meteoric waters is highlighted by the d-excess plot in Figure 5 where the seasonal ice range extends below the summer precipitation range along a slope that is clearly different than the approximately zero slopes of the precipitation fields. The seasonal ice trend is consistent with freeze-out fractionation. When this process occurs, a characteristic inverse (negative) linear relationship occurs between d-excess and corresponding δ values (either δ^2H or $\delta^{18}O$) (Souchez et al., 2000; Fritz et al., 2011). d-excess is useful to visually represent fractionation during freezing and can support interpretation of water sources from ice melt as we demonstrate here (see Lacelle, 2011, for a review). d-excess values are affected by conditions during freezing (rate of freezing, boundary layer thickness and percentage of reservoir freezing), and a more negative

slope for *d*-excess *versus* $\delta^{18}O$ occurs for waters with a more negative initial isotopic composition prior to freezing (Souchez *et al.*, 2000). *d*-excess *versus* $\delta^{18}O$ values for our active layer ice samples plotted with a linear correlation ($r^2 = 0.39$) $d\text{-excess} = -2.3 * \delta^{18}O - 31.9$ (Figure 6a), suggesting that freezing occurred either under a closed system (with no new/continuous water inputs) or in an open system with new water inputs having the same isotopic composition as existing water (Souchez *et al.*, 2000; Fritz *et al.*, 2011). The second condition is doubtful given the lack of evidence for significant wintertime lateral flow in polygonal ground and because any new precipitation inputs during winter would be snow.

It needs to be emphasized that the fractionation effects that occur for evaporation and freeze-out fractionation are isotopically indistinguishable (Figure 6a and b). We observed similar isotopic fractionation effects in seasonal ice (and textural permafrost, as discussed in the following section) as in July surface waters (Figure 6a and b). It is unlikely, however, that the low-*d*-excess ice samples represent frozen, previously evaporated, water. As discussed earlier, evaporation effects are strongest earlier in the summer, and by September, little to no evaporative signature remains. Thus, the isotope composition of water prior to freeze-up is unlikely to have an evaporated signature. Instead, it is much more likely that the seasonal ice values have been affected by freeze-out fractionation effects. Isotopic fractionation occurring during freeze-out has been documented for ground ice and rivers (e.g. Gibson and Prowse, 2002; Brosius *et al.*, 2012), and it appears that ground ice in polygonal ground is also affected by this process. Freeze-out-affected values may also be useful in helping differentiate melting seasonal ice from within-year meteoric sources.

Freeze-out fractionation occurs during freezing of water due to diffusion kinetics. During this process, water molecules containing deuterium or oxygen-18 preferentially freeze out of solution before their lighter counterparts. Instead of representing the isotopic values of the water just prior to freeze-up, freeze-out fractionation results in ice depth profiles where the first ice to freeze will have less negative isotope compositions and later ice will have progressively more negative isotope compositions (Souchez *et al.*, 2000). Active layer freeze-up in Barrow occurs top-down and bottom-up, creating closed or semi-closed conditions that promote freeze-out fractionation. Freeze-out fractionation has been previously noted in arctic ice cores to produce a linear slope of δ^2H *versus* $\delta^{18}O$ shallower than the MWL (Souchez *et al.*, 2000; Fritz *et al.*, 2011). Just as with an evaporation slope, the intersection of a freezing slope with the MWL indicates the isotopic composition of the original bulk water source prior to freezing (Souchez *et al.*, 2000). We were able to use the intercepts from five

study site ice cores (cores not containing ice wedge material) to calculate theoretical freeze-out slopes for our site using the closed system model of Jouzel and Souchez (1982). Values were similar for all cores and ranged from 5.5 to 5.7, further demonstrating the similarity between surface water evaporation (typically slopes of 4–6) and freeze-out on isotope compositions. Slopes calculated using regressions of the individual core isotope values ranged from 2 to 6.5 with an average of 5.2 (some cores had small numbers of samples, which likely explains some of the variation). The regression equation for all seasonal ice samples was $\delta^2H = 5.7 * \delta^{18}O - 31.7$ ($R^2 = 0.79$), intercepting the LMWL at $\delta^2H = -150.45$ and $\delta^{18}O = -17.12$ (Figure 4c). This intercept is within the field for fall precipitation and also indicates the isotopic composition that would occur for seasonal ice that melted and completely homogenized.

There is only one active layer sample that shows an unusually low *d*-excess value compared with meteoric sources (Figure 5). This sample is from shallow pore water, which suggests the low *d*-excess might be from evaporation as opposed to freeze-out (although given the similar effect of these processes on isotopic compositions, a definitive conclusion is not possible). In any case, there does not appear to be any clear indication that freeze-out-affected ice melt contributes significantly as a source to the active layer, despite the fact we physically know that at least some portion must be from recently melted seasonal ice. There are a couple of possibilities to explain the lack of an apparent freeze-out-affected ice contribution. First, because deepening of the active layer occurs slowly over multiple months, the ice melt contribution could be small enough over short timescales that incoming precipitation rates essentially dominate the active layer water balance, thus swamping the freeze-out signal. Alternatively, if ice melt homogenizes enough, mixing out the isotopic depth variations present in an ice profile, the isotopic composition will converge on the value of water just prior to freeze-up, and the isotopic fractionation effect is lost (see discussion in Boereboom *et al.*, 2013, about depth scaling and homogenization). The homogenization explanation seems unlikely given that the depth variations in isotope and geochemical compositions in the active layer suggest a poorly mixed system. In the end, it is difficult to estimate the ice melt contribution using isotopes alone. Overall, it appears that fall and summer precipitation sources are the most significant contributors of moisture to the active layer and that seasonal ice melt may represent a secondary component.

Mixing model results (Table III) also suggest that fall and summer precipitations are the dominant sources of active layer water, representing 57–82% of the total depending on sample type. The mixing model takes into account

deviations from the MWL introduced from freeze-out fractionation. Thus, estimates are effectively based on an assumption of unhomogenized meltwater in the active layer and likely represent *minimum* ice melt contributions. The model does suggest that, while summer/fall contributions are dominant, ice melt sources are important. Estimates of winter/spring contributions via snowmelt are also substantial for the centres of high-centred polygons (above the water table) and deep samples (near the frost line). However, for reasons discussed earlier, we suspect these winter/spring contributions are overestimates. For example, it is clear from Figure 5 that one can explain all of the high-centred polygon data (+WT) as having a 100% fall precipitation source. This issue highlights a limitation of most statistical mixing model approaches in that they will assign some contribution to all sources regardless of whether the data can be explained by a lesser number of sources.

Textural and ice wedge permafrost versus active layer ice

Although the main focus of this study was on active layer waters and seasonal ice, it is also worthwhile to examine the stable isotope composition of associated permafrost. Conceptual models for permafrost formation propose that different mechanisms and sources contribute to the formation of textural *versus* massive ice permafrost (e.g. ice wedges). Evidence suggests that textural ice forms from mainly summer precipitation infiltration and resident active layer pore waters, while wedge ice occurs when winter thermal contraction cracking allows percolation and subsequent freezing of isotopically depleted winter precipitation during spring melt (e.g. Meyer *et al.*, 2010a; Brosius *et al.*, 2012). While there was some overlap in our study for water stable isotope values between textural and wedge ice permafrost samples, wedge ice samples had significantly depleted water isotope signatures and plotted primarily within the winter precipitation field (Figure 4c). Wedge ice also did not show evidence of freeze-out fractionation effects (Figure 6a). In contrast, textural permafrost ice samples plotted with a freeze-out slope intersecting the LMWL within the summer precipitation field (Figure 4c). Overlap of some ice wedge and textural ice samples could be due to exchange and mixing of wedge ice with sediment, which has been previously observed in palaeoclimate studies at the interface between ice wedges and textural ice (Meyer *et al.*, 2010a and 2010b). Despite some evidence for mixing, our results are consistent with the accepted model of a summer precipitation source for textural ice and a winter precipitation source for wedge ice based on the respective precipitation source fields (Figures 4c and 6a). The freeze-out fractionation effect for textural ice was particularly apparent from the plot of *d*-excess *versus* $\delta^{18}O$, with a strong linear regression ($r^2 = 0.70$) *d*-excess $= -0.29 * \delta^{18}O - 14.1$, which did not

occur for wedge ice ($r^2 = 0.20$; Figure 6a). The lack of a freeze-out fractionation effect for wedge ice has been noted in other studies (Fritz *et al.*, 2011) and is consistent with accepted mechanisms for wedge ice formation that suggest open-system freezing due to repeated additions of winter precipitation forming thin ice layers (Brosius *et al.*, 2012; Vasil'chuk, 2013). As a result, water stable isotopes of ice wedges are commonly used to provide proxy data for palaeoclimatic and palaeoenvironmental reconstructions (Gibson and Prowse, 2002; Meyer *et al.*, 2010a, b; Boereboom *et al.*, 2013; Iwahana *et al.*, 2014) and thaw unconformities (Lacelle *et al.*, 2014).

Notable similarities are apparent for seasonal ice *versus* textural permafrost ice in the plots of δ^2H and $\delta^{18}O$ and *d*-excess *versus* $\delta^{18}O$ (Figures 4c and 6), suggesting similar water sources and similar freezing conditions for modern active layer and shallow (<1 m) textural permafrost ice. Carbon-14 dating indicates Holocene ages for the shallow permafrost zone (Hinkel *et al.*, 2003; Meyer *et al.*, 2010b).

SUMMARY

Run-off in temperate mid-latitude regions is relatively well characterized, but in high-latitude arctic regions, there are few hydrologic studies that have examined stable isotopes from active layer pore waters during the warm season to infer sources and cycling. Thus, sources of active layer waters are not well understood, and the variation of seasonal precipitation inputs is unclear (Ali *et al.*, 2015). To our knowledge, this is the first study to examine water sources to active layer pore waters in a polygonal tundra landscape using water stable isotopes. Although there are still some uncertainties, our results support a generalized conceptual model of sources of water to the active layer in polygonal ground (Figure 7). The active layer stable isotope values indicate a lack of winter/spring precipitation contributions, suggesting that most of the snowmelt pulse quickly runs off the landscape, consistent with field observations at our study site and other arctic watershed studies (left side of diagram). By August, the isotope data suggest that summer rain is likely the most prominent active layer water source (middle of diagram). There is also good evidence for evaporative fractionation of surface and shallow subsurface waters in early summer to midsummer. In September, there are strong indications of substantial fall precipitation contributions, and some contributions of melting active layer seasonal ice are likely. One limitation of this study is that it was difficult to constrain the ice melt contribution. Mixing model results suggest ice melt can be an important, but not dominant, source. By September, little to no evaporation effect is evident in active layer waters. By October, freeze-up typically begins (right side of the diagram) and
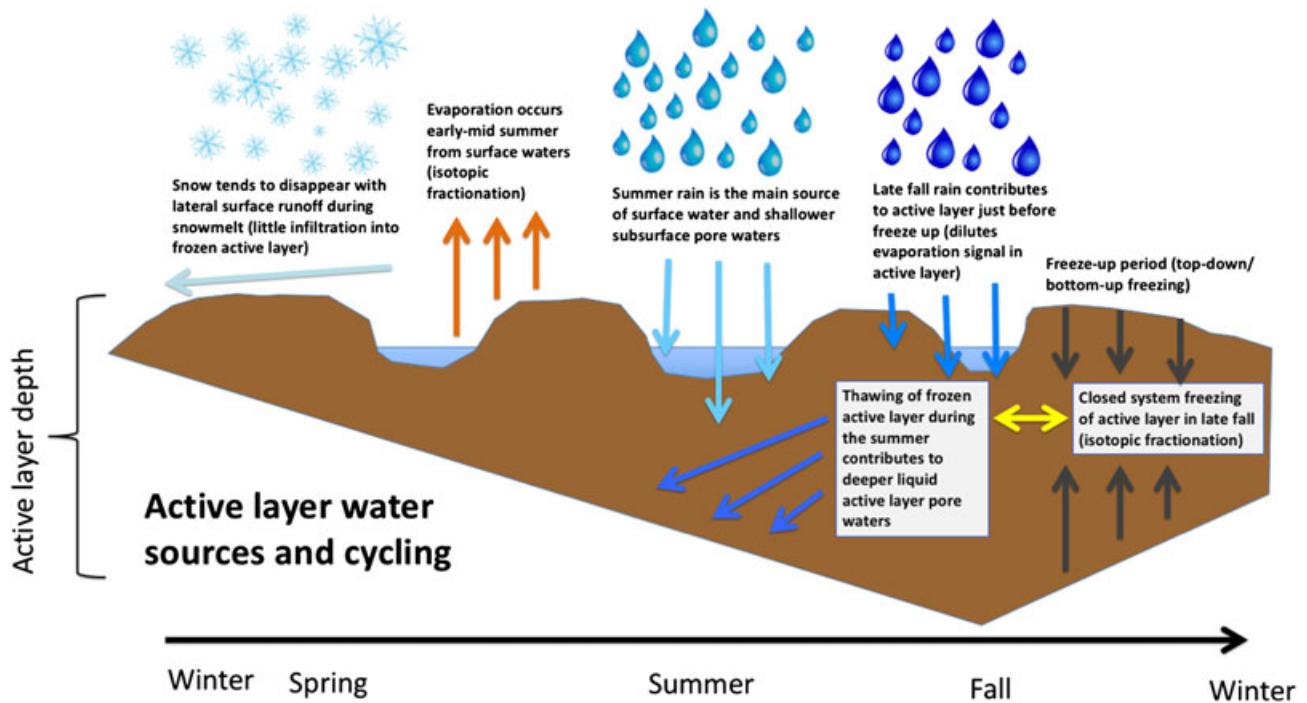
Figure 7. Conceptual diagram of active layer water sources and seasonal cycling

occurs from both the surface downward and the bottom of the active layer upward (although not necessarily at the same rate). This process results in a closed or semi-closed condition that promotes freeze-out fractionation of the isotopes. Depth profiles of seasonal ice commonly showed deviations from the MWL and *d*-excess values that are consistent with freeze-out fractionation. However, little evidence was found for freeze-out-fractionated melt in the active layer samples. Aspects of this conceptual model need further testing and thus should be useful for developing hypotheses and to help guide future studies of active layer isotopes and water sources.

Although uncertainties remain, this study demonstrates that the application of stable isotopes is a useful tool that can help identify sources of water in the active layer and act as an indicator of processes such as evaporation (Craig, 1961; Gonfiantini, 1986) and freeze-out fractionation in polygonal ground. Both evaporation and freeze-out fractionation may result in isotopic fractionation with a δ^2H *versus* $\delta^{18}O$ regression slope shallower than the MWL, providing an opportunity to make inferences about hydrologic conditions and processes. In particular, we demonstrate the utility of *d*-excess to provide additional insight into both freeze-out fractionation and evaporation, which were highly apparent in the graphical representation of *d*-excess plotted against $\delta^{18}O$. Our field data support theoretical studies that the isotopic fractionation that occurs for freeze-out fractionation and evaporation is essentially indistinguishable in their slopes and fractionation effects. Thus, interpretation of water isotopes in

seasonally frozen systems will need to utilize other information besides the isotope composition of a particular sample to infer which process is actually occurring.

In addition to the active layer, we also examined stable isotopes in shallow permafrost. Unlike textural permafrost and active layer ice, which had summer rain sources, wedge ice had a largely winter precipitation source. Further, freeze-out fractionation was not evident in wedge ice, suggesting open-system freezing with continuous inputs of winter precipitation forming thin ice layers. Both sources and mechanisms of textural and wedge ice are consistent with different water sources and mechanisms of formation (Brosius *et al.*, 2012; Vasil'chuk, 2013).

In conclusion, the hydrology of polygonal ground is a strong control on active layer biogeochemistry, nutrient availability and CO_2 and CH_4 production in arctic systems (e.g. Heikoop *et al.*, 2015; Newman *et al.*, 2015; Throckmorton *et al.*, 2015). These results provide additional insights into active layer water sources and cycling in a polygonal tundra landscape that will be critical to addressing uncertainties and building better regional or pan-arctic hydrological and biogeochemical models.

REFERENCES

Aleina FC, Brovkin V, Muster S, Boike J, Kutzbach L, Sachs T, Zuyev S. 2013. A stochastic model for the polygonal tundra based on Poisson–Voronoi diagrams. *Earth System Dynamics* **4**: 187–198. DOI:10.5194/Esd-4-187-2013

Alexandrov BS, Vesselinov VV. 2014. Blind source separation for groundwater pressure analysis based on nonnegative matrix factorization. *Water Resources Research* **50**(9): 7332–7347.

Ali G, Tetzlaff D, McDonnel JJ, Soulsby C, Carey S, Laudon H, McGuire K, Buttle J, Shanley J. 2015. Comparison of threshold hydrologic response across northern catchments. *Hydrological Processes* **29**: 3575–3591.

Anderson L, Birks J, Rover J, Guldager N. 2013. Controls on recent Alaskan lake changes identified from water isotopes and remote sensing. *Geophysical Research Letters* **40**: 3413–3418. DOI:10.1002/Grl.50672

Arp CD, Jones BM, Urban FE, Grosse G. 2011. Hydrogeomorphic processes of thermokarst lakes with grounded-ice and floating-ice regimes on the Arctic coastal plain, Alaska. *Hydrological Processes* **25**: 2422–2438. DOI:10.1002/Hyp.8019

Atchley AL, Painter SL, Harp DR, Coon ET, Wilson CJ. 2015. Using field observations to inform thermal hydrology models of permafrost dynamics with ATS (v0.83). *Geoscientific Model Development* **8**: 2701–2722.

Barnes CJ, Allison GB. 1983. The distribution of deuterium and ^{18}O in dry soils, 1. *Theory Journal Hydrology* **60**: 141–156.

Billings WD, Peterson KM. 1980. Vegetational change and ice-wedge polygons through the thaw-lake cycle in arctic Alaska. *Arctic Alpine Research* **12**: 413–432. DOI:10.2307/1550492

Blaen PJ, Hannah DM, Brown LE, Milner AM. 2014. Water source dynamics of high arctic river basins. *Hydrological Processes* **28**: 3521–3538. DOI:10.1002/hyp.9891

Bockheim JG, Hinkel KM. 2005. Characteristics and significance of the transition zone in drained thaw-lake basins of the Arctic Coastal Plain, Alaska. *Arctic* **58**: 406–417.

Bockheim JG, Hinkel KM, Eisner WR, Dai XY. 2004. Carbon pools and accumulation rates in an age-series of soils in drained thaw-lake basins, Arctic Alaska. *Soil Science Society of America Journal* **68**: 697–704.

Boereboom T, Samyn D, Meyer H, Tison JL. 2013. Stable isotope and gas properties of two climatically contrasting (Pleistocene and Holocene) ice wedges from Cape Mamontov Klyk, Laptev Sea, northern Siberia. *The Cryosphere* **7**: 31–46. DOI:10.5194/Tc-7-31-2013

Boike J, Wille C, Abnizova A. 2008. Climatology and summer energy and water balance of polygonal tundra in the Lena River Delta, Siberia. *Journal of Geophysical Research: Biogeosciences* **113**. DOI: Artn G03025: DOI:10.1029/2007jg000540

Bowling LC, Kane DL, Gieck RE, Hinzman LD, Lettenmaier DP. 2003. The role of surface storage in a low-gradient arctic watershed. *Water Resources Research* **39**. DOI: Artn 1087: DOI:10.1029/2002wr001466

Brosius LS, Anthony KMW, Grosse G, Chanton JP, Farquharson LM, Overduin PP, Meyer H. 2012. Using the deuterium isotope composition of permafrost meltwater to constrain thermokarst lake contributions to atmospheric CH_4 during the last deglaciation. *Journal of Geophysical Research: Biogeosciences* **117**. DOI: Artn G01022: DOI:10.1029/2011jg001810

Cooper LW, Olsen CR, Solomon DK, Larsen IL, Cook RB, Grebmeier JM. 1991. Stable isotopes of oxygen and natural and fallout radionuclides used for tracing runoff during snowmelt in an arctic watershed. *Water Resources Research* **27**: 2171–2179. DOI:10.1029/91wr01243

Craig H. 1961. Isotopic variations in meteoric waters. *Science* **133**: 1702–1703.

Dansgaard W. 1964. Stable Isotopes in precipitation. *Tellus* **16**: 436–468.

Dunning I, Huchette J, Lubin M. 2015. JuMP: a modeling language for mathematical optimization. *arXiv preprint arXiv:1508.01982*.

Fiedler S, Wagner D, Kutzbach L, Pfeiffer EM. 2004. Element redistribution along hydraulic and redox gradients of low-centered polygons, Lena Delta, northern Siberia. *Soil Science Society of America Journal* **68**: 1002–1011.

French H. 2007. *The Periglacial Environment*, 3rd edition. Wiley: West Sussex, England.

Frisbee MD, Phillips FM, Campbell AR, Hendrickx JMH. 2010. Modified passive capillary samplers for collecting samples of snowmelt infiltration for stable isotope analysis in remote, seasonally inaccessible watersheds 1: laboratory evaluation. *Hydrological Processes* **24**: 825–833. DOI:10.1002/hyp.7523

Fritz M, Wetterich S, Meyer H, Schirrmeister L, Lantuit H, Pollard WH. 2011. Origin and characteristics of massive ground ice on Herschel Island (Western Canadian Arctic) as revealed by stable water isotope and hydrochemical signatures. *Permafrost and Periglacial* **22**: 26–38. DOI:10.1002/ppp.714

Gibson JJ, Prowse TD. 2002. Stable isotopes in river ice: identifying primary over-winter streamflow signals and their hydrological significance. *Hydrological Processes* **16**: 873–890.

Gonfiantini R. 1986. Environmental isotopes in lake studies. In *Handbook of Environmental Isotope Geochemistry. The Terrestrial Environment, B*, Fritz P, Fontes J-C (eds), **2**. Elsevier: Amsterdam, The Netherlands; 113–168.

Heikoop JM, Throckmorton HM, Newman BD, Perkins GB, Iversen CM, Roy Chowdhury T, Romanovsky V, Graham DE, Norby RJ, Wilson CJ, Wullschleger SD. 2015. Isotopic identification of soil and permafrost nitrate sources in an Arctic tundra ecosystem. *Journal of Geophysical Research: Biogeosciences* **120**: 1000–1017.

Helbig M, Boike J, Langer M, Schreiber P, Runkle BRK, Kutzbach L. 2013. Spatial and seasonal variability of polygonal tundra water balance: Lena River Delta, northern Siberia (Russia). *Hydrogeology Journal* **21**: 133–147.

Hinkel KM, Eisner WR, Bockheim JG, Nelson FE, Peterson KM, Dai XY. 2003. Spatial extent, age, and carbon stocks in drained thaw lake basins on the Barrow Peninsula, Alaska. *Arctic Antarctic and Alpine Research* **35**: 291–300. DOI:10.1657/1523-0430(2003)035[0291:Seaacs]2.0.Co;2

IAEA/WMO. 2015. Global network of isotopes in precipitation. The GNIP database. Accessible at: http://www.iaea.org/water

Iwahana G, Takano S, Petrov RE, Tei S, Shingubara R, Maximov TC, Fedorov AN, Desyatkin AR, Nikolaev AN, Desyatkin RV, Sugimoto A. 2014. Geocryological characteristics of the upper permafrost in a tundra-forest transition of the Indigirka River Valley, Russia. *Polar Science* **8**: 96–113. DOI:10.1016/j.polar.2014.01.005

Jouzel J, Souchez RA. 1982. Melting-refreezing at the glacier sole and the isotopic composition of the ice. *Journal of Glaciology* **28**: 35–42.

Koch JC, Gurney K, Wipfli MS. 2014. Morphology-dependent water budgets and nutrient fluxes in arctic thaw ponds. *Permafrost and Periglacial* **25**: 79–93. DOI:10.1002/ppp.1804

Lacelle D. 2011. On the delta O-18, delta d and d-excess relations in meteoric precipitation and during equilibrium freezing: theoretical approach and field examples. *Permafrost and Periglacial* **22**: 13–25. DOI:10.1002/ppp.712

Lacelle D, Fontaine M, Forest AP, Kokelj S. 2014. High-resolution stable water isotopes as tracers of thaw unconformities in permafrost: a case study from western arctic Canada. *Chemical Geology* **368**: 85–96. DOI:10.1016/j.chemgeo.2014.01.005

Lee DD, Seung SH. 1999. Learning the parts of objects by non-negative matrix factorization. *Nature* **401**(6755): 788–791.

Liljedahl AK, Hinzman LD, Harazono Y, Zona D, Tweedie CE, Hollister RD, Engstrom R, Oechel WC. 2011. Nonlinear controls on evapotranspiration in arctic coastal wetlands. ▪▪▪▪ **8**: 3375–3389.

Marsh P. 1999. Snowcover formation and melt: recent advances and future prospects. *Hydrological Processes* **13**: 2117–2134.

Mendez J, Hinzman LD, Kane DL. 1998. Evapotranspiration from a wetland complex on the Arctic Coastal Plain of Alaska. *Nordic Hydrology* **29**: 303–330.

Meyer H, Schirrmeister L, Andreev A, Wagner D, Hubberten HW, Yoshikawa K, Bobrov A, Wetterich S, Opel T, Kandiano E, Brown J. 2010a. Late Glacial and Holocene isotopic and environmental history of northern coastal Alaska—results from a buried ice-wedge system at Barrow. *Quaternary Science Review* **29**: 3720–3735. DOI:10.1016/j.quascirev.2010.08.005

Meyer H, Schirrmeister L, Yoshikawa K, Opel T, Wetterich S, Hubberten HW, Brown J. 2010b. Permafrost evidence for severe winter cooling during the Younger Dryas in northern Alaska. *Geophysical Research Letters* **37**. DOI: Artn L03501: DOI:10.1029/2009gl041013

Natali SM, Schuur EA, Mauritz M, Schade JD, Celis G, Crummer KG, Johnston C, Krapek J, Pegoraro E, Salmon VG, Webb EE. 2015. Permafrost thaw and soil moisture driving CO_2 and CH_4 release from upland tundra. *Geophysical Research Letters* **3**: 525–537. DOI:10.1002/2014JG002872

Newman BD, Campbell AR, Wilcox BP. 1998. Lateral subsurface flow pathways in a semiarid ponderosa pine hillslope. *Water Resources Research* **34**: 3485–3496.

Newman BD, Throckmorton HM, Graham DE, Gu B, Hubbard SS, Liang L, Wu Y, Heikoop JM, Herndon EM, Phelps TJ, Wilson CJ, Wullschleger SD. 2015. Microtopographic and depth controls on active layer chemistry in arctic polygonal ground. *Geophysical Research Letters* **42**: 1808–1817. DOI:10.1002/2014gl062804

Painter SL, Moulton JD, Wilson CJ. 2013. Modeling challenges for predicting hydrologic response to degrading permafrost. *Hydrogeology Journal* **21**: 221–224. DOI:10.1007/S10040-012-0917-4

Quinton WL, Gray DM, Marsh P. 2000. Subsurface drainage from hummock-covered hillslopes in the Arctic tundra. *Journal of Hydrology* **237**: 113–125.

Quinton WL, Hayashi M, Carey SK. 2008. Peat hydraulic conductivity in cold regions and its relation to pore size and geometry. *Hydrological Processes* **22**: 2829–2837.

Quinton WL, Marsh P. 1998. The influence of mineral earth hummocks on subsurface drainage in the continuous permafrost zone. *Permafrost and Periglacial Processes* **9**: 213–228.

Seeberg-Elverfeldt J, Schluter M, Feseker T, Kolling M. 2005. *Rhizon sampling of porewaters near the sediment-water interface of aquatic systems*. Limnology and Oceanography: Methods; 361–371.

Souchez R, Jouzel J, Lorrain R, Sleewaegen S, Stievenard M, Verbeke V. 2000. A kinetic isotope effect during ice formation by water freezing. *Geophysical Research Letters* **27**: 1923–1926. DOI:10.1029/2000gl006103

Streletskiy DA, Tananaev NI, Opel T, Shiklomanov NI, Nyland KE, Streletskaya ID, Shiklomanov AI. 2015. Permafrost hydrology in changing climatic conditions: seasonal variability of stable isotope composition in rivers in discontinuous permafrost. *Environmental Research Letters* **10**(9): 095003.

Sugimoto A, Naito D, Yanagisawa N, Ichiyanagi K, Kurita N, Kubota J, Kotake T, Ohata T, Maximov TC, Fedorov AN. 2003. Characteristics of soil moisture in permafrost observed in East Siberian taiga with stable isotopes of water. *Hydrological Processes* **17**: 1073–1092.

Takata K, Kimoto M. 2000. A numerical study on the impact of soil freezing on the continental-scale seasonal cycle. *Journal of the Meteorological Society of Japan* **78**: 199–221.

Tetzlaff D, Buttle J, Carey SK, van Huijgevoort MHJ, Laudon H, McNamara JP, Mitchell CPJ, Spence C, Gabor RS, Soulsby C. 2015a. A preliminary assessment of water partitioning and ecohydrological coupling in northern headwaters using stable isotopes and conceptual runoff models. *Hydrological Processes* **29**: 5153–5173.

Tetzlaff D, Buttle J, Carey S, McGuire K, Laudon H, Soulsby C. 2015b. Tracer-based assessment of low paths, storage and runoff generation in northern catchments: a review. *Hydrological Processes* **29**: 3475–3490.

Throckmorton H, Perkins G, Altmann G, Muss J, Smith L, Conrad M, Torn M, Heikoop J, Newman B, Wilson C, Wullschleger S. 2015. Pathways and transformations of dissolved methane and dissolved inorganic carbon in Arctic tundra soils: evidence from analysis of stable isotopes. *Global Biogeochemical Cycles* **29**(11): 1893–1910.

Throckmorton H, Wilson C, Heikoop J, Newman B. 2016. Geochemical and isotopic water results, Barrow, Alaska, 2012-2013 (2012 synoptic data and the d18O and the dD data). *Next Generation Ecosystem Experiments Arctic Data Collection, Carbon Dioxide Information Analysis Center*. Oak Ridge National Laboratory: Oak Ridge, Tennessee, USA. Data set accessed at DOI:10.5440/1164892

Vasil'chuk YK. 2013. Syngenetic ice wedges: cyclical formation, radiocarbon age and stable isotope records. *Permafrost and Periglacial Processes* **24**: 82–93.

Walvoord MA, Voss CI, Wellman TP. 2012. Influence of permafrost distribution on groundwater flow in the context of climate-driven permafrost thaw: example from Yukon Flats Basin, Alaska, United States. *Water Resources Research* **48**. DOI: Artn W07524: DOI:10.1029/2011wr011595

Woo MK, Kane DL, Carey SK, Yang DQ. 2008. Progress in permafrost hydrology in the new millennium. *Permafrost and Periglacial* **19**: 237–254. DOI:10.1002/ppp.613

Zhang Z, Kane DL, Hinzman LD. 2000. Development and application of a spatially-distributed arctic hydrological and thermal process model (ARHYTHM). *Hydrological Processes* **14**: 1017-+. DOI:10.1002/(Sici)1099-1085(20000430)14:6<1017::Aid-Hyp982>3.0.Co;2-G

Zona D, Oechel WC, Peterson KM, Clements RJ, Pawu KT, Ustin SL. 2010. Characterization of the carbon fluxes of a vegetated drained lake basin chronosequence on the Alaskan Arctic Coastal Plain. *Global Change Biology* **16**: 1870–1882. DOI:10.1111/J.1365-2486.2009.02107.X

SUPPORTING INFORMATION

Additional supporting information may be found in the online version of this article at the publisher's web-site.